

⁹K. W. Taconis and R. de Bruyn Ouboter, in *Progress in Low-Temperature Physics*, edited by C. J. Gorter (North-Holland Publishing Company, Amsterdam, The Netherlands, 1964), Vol. 4, Chap. II.

¹⁰H. C. Kramers, J. D. Wasscher, and C. J. Gorter, *Physica* **18**, 329 (1952).

¹¹I. M. Khalatnikov, *Introduction to the Theory of Superfluidity* (W. A. Benjamin, Inc., New York, 1965).

¹²J. E. Opfer, Ph. D. thesis, Washington University, 1966 (unpublished).

¹³T. P. Ptukha, *Z. Eksperim. i Teor. Fiz.* **40**, 1583 (1961) [English transl.: *Soviet Phys. - JETP* **13**, 1112 (1961)].

¹⁴I. M. Khalatnikov and V. N. Zharkov, *Z. Eksperim. i Teor. Fiz.* **32**, 1108 (1957) [English transl.: *Soviet Phys. -*

JETP **5**, 905 (1957)].

¹⁵D. G. Henshaw and A. D. B. Woods, *Phys. Rev.* **121**, 1266 (1961); *Proceedings of the Seventh International Conference on Low-Temperature Physics*, edited by G. M. Graham and A. C. Hollis-Hallet (University of Toronto, 1961), p. 539.

¹⁶L. Meyer and F. Reif, *Phys. Rev. Letters* **5**, 1 (1960); *Phys. Rev. Letters* **119**, 1164 (1960).

¹⁷R. Abe and K. Aizu, *Phys. Rev.* **123**, 10 (1961).

¹⁸V. N. Grigor'ev, B. N. Esel'son, V. P. Mal'khanov, and V. I. Sobolev, *Z. Eksperim. i Teor. Fiz.* **51**, 1059 (1966) [English transl.: *Soviet Phys. - JETP* **24**, 707 (1967)].

Recombination, Attachment, and Ambipolar Diffusion of Electrons in Photo-Ionized NO Afterglows*

Charles S. Weller[†] and Manfred A. Biondi
*Department of Physics, University of Pittsburgh,
 Pittsburgh, Pennsylvania*
 (Received 11 March 1968)

Photo-ionized plasma afterglows of NO have been studied by combined microwave and mass-spectrometric techniques. Nitric-oxide-neon mixtures (5–65 mTorr NO, 2–7 Torr Ne) are contained in a 10-cm resonant cavity where they are ionized by a “single pulse” of Lyman- α radiation. A temporal spectrum of ions diffusing to the wall is obtained by a differentially pumped mass spectrometer and multichannel analyzer. Analysis of the electron-density decay curves obtained by microwave techniques to obtain an electron-ion recombination coefficient for NO⁺ is complicated by the conversion of NO⁺ to the dimer ion, (NO)₂⁺. At sufficiently low densities of nitric oxide the (NO)₂⁺ concentration becomes negligible, and the NO⁺ wall current tracks the electron-density decay. From comparisons of experimental electron-density decay curves obtained under recombination-controlled conditions, with computer solutions of the electron-continuity equation, the values $\alpha(\text{NO}^+) = (7.4 \pm 0.7)$, (4.1 ± 0.3) , and $(3.1 \pm 0.2) \times 10^{-7}$ cm³/sec, at $T = 200, 300,$ and 450°K , respectively, are obtained. From analysis of electron-density decay curves at higher densities of NO, where (NO)₂⁺ is the dominant ion, the value $\alpha(\text{NO})_2^+ = (1.7 \pm 0.4) \times 10^{-6}$ cm³/sec at $T = 300^\circ\text{K}$ is obtained. The three-body electron-attachment and ambipolar diffusion coefficients have been measured in pure NO (0.1–5 Torr) and are found to be $K = (1.3 \pm 0.1) \times 10^{-31}$ cm⁶/sec and $D_a \rho = 80 \pm 16$ cm² Torr/sec, respectively, at $T = 300^\circ\text{K}$.

I. INTRODUCTION

The principal interest in electron removal processes in nitric oxide plasmas stems from the important role the NO⁺ ion plays in the earth's ionosphere. Although the neutral NO molecule is a minor species in the upper atmosphere, NO⁺ is an important atmospheric ion.^{1,2} Since NO has the lowest ionization potential of the atmospheric gases, the NO⁺ ion usually cannot react further with the ionic and neutral species present, but must wait to recombine with a free electron (or, possibly, a negative ion) in order to be neutralized.

The rate of recombination between NO⁺ ions and electrons may be expected to vary with the temperature of the ions and of the electrons. Over the ionospheric regions of interest, the neutral-gas and ion temperatures vary from approximately 200 to over 1000°K.³ The electron temperature above about 150 km has been shown to be greater

than the ion temperature by as much as several hundred degrees.⁴ As a result, laboratory experiments should include an extensive range of ion and electron temperatures in order that the measured rates will be applicable to all regions of the ionosphere where recombination of electrons with NO⁺ ions is important.

The NO⁺ ion in the ionosphere is expected to be in its ground electronic state. In the *D* region, where it is produced by Lyman- α photoionization, this is a certainty. In the *E* and *F* regions, where the NO⁺ ion is produced by ion-molecule reactions, energy considerations require that it be in its ground electronic state, unless the primary ion (e.g., N₂⁺ or O₂⁺) in the reaction is electronically or vibrationally excited. However, there is no evidence for such an excited-ion population in the ionosphere. Unfortunately, at present nothing can be said about the vibrational state of the NO⁺ ion in the ionosphere.

The present experiment was undertaken to produce a plasma of NO^+ ions and electrons in a suitable apparatus in the laboratory and then to measure the rates of decay of electron density and of mass-analyzed ion wall currents under recombination-controlled afterglow conditions. These measurements provide determinations of the rates of electron-ion recombination and other relevant processes. In addition, measurements have been made over a range of ion-electron-neutral-gas temperatures in order to obtain the temperature dependence of the electron-ion recombination coefficient.

II. APPARATUS AND MEASUREMENTS

Figure 1 is a simplified diagram of the experimental apparatus. Highly purified nitric oxide gas and purified research-grade neon gas as a buffer gas are contained in a cylindrical copper microwave cavity (resonating at ~ 3 GHz). The cavity is part of a bakeable ultrahigh vacuum system. To avoid dissociation of NO with subsequent reactions to form undesirable species such as NO_2 , photoionization instead of the usual microwave discharge is used to create the plasma. A pulse (~ 0.5 msec) of radiation in the neighborhood of Lyman α ($h\nu = 10.23$ eV) produced by a hydrogen flash lamp creates an NO^+ ion (9.25 eV) in the ground electronic state and in the first few vibrational levels, which is the expected state of the NO^+ ion in the ionosphere. The photoelectrons produced in the photo-ionization process are released with up to 2 eV of kinetic energy; however, they are rapidly thermalized. A simple elastic-collision model calculation gives thermalization times in the range of 5–50 μsec for the range of gas densities used in the experiment. This is a negligible amount of time on the time scale of the measurements, and so the electrons are effectively always at the temperature of the ions and neutrals.

The principal measurement in this experiment is that of the electron density as a function of time. This is accomplished by microwave techniques,⁵ in which the presence of free electrons within a microwave cavity changes its resonant frequency from the normal "empty" value. The shift in resonant frequency, Δf , has been shown to be

$$\Delta f(t) \approx \frac{e^2}{4\pi m f_0 \epsilon_0} \frac{\int_V n_e(\vec{r}, t) E_0^2(\vec{r}) dV}{\int_V E_0^2(\vec{r}) dV}, \quad (1)$$

where e and m are the charge and mass of the electron, respectively; f_0 is the "empty" resonant frequency of the cavity; ϵ_0 is the permittivity of free space; $n_e(\vec{r}, t)$ is the electron density as a function of space and time; and $E_0(\vec{r})$ is the amplitude of the probing microwave electric field as a function of position. We introduce the "microwave field-weighted average" electron density, $\bar{n}_{\mu w}$, by

$$\bar{n}_{\mu w}(t) \equiv \frac{\int_V n_e(\vec{r}, t) E_0^2(\vec{r}) dV}{\int_V E_0^2(\vec{r}) dV} = \frac{4\pi m f_0 \epsilon_0}{e^2} \Delta f(t); \quad (2)$$

that is, $\bar{n}_{\mu w}$ is the experimentally measured frequency shift multiplied by some physical constants. (It is this quantity that will be discussed in the analysis of the experiment in Sec. IV.)

The time dependence of mass-identified ion currents which diffuse to the walls of the vessel is also studied in this experiment. To do this, there is a small (0.010 in. diam) sampling orifice in the plane wall of the cavity (see Fig. 1). Ions which

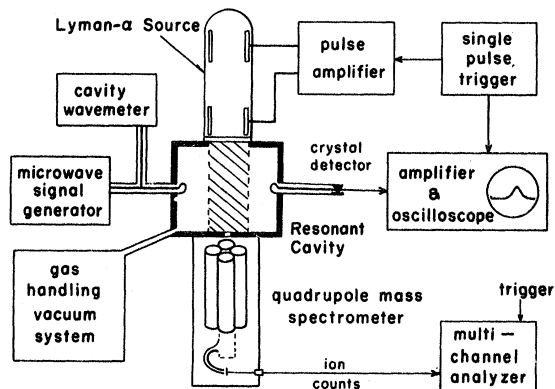


FIG. 1. Simplified block diagram of the combined microwave-mass-spectrometric afterglow apparatus employing photoionization.

pass through the orifice are drawn by a uniform electric field into a quadrupole mass filter.⁶ The mass-selected ions then impinge upon a Channeltron⁷ electron-multiplying device, whose output pulses are entered into a multichannel analyzer operating in a multiscaling mode. In this manner the time dependence of mass-selected ion wall currents is obtained.

Considering an afterglow containing only NO^+ ions and electrons, the NO^+ wall current density is given by

$$\vec{\Gamma}_{\text{wall}}^+ = -D_a [\nabla n_+(\vec{r}, t)]_{\text{wall}}, \quad (3)$$

where D_a is the ambipolar coefficient of the electrons and ions, of density n_e and n_+ , respectively. Now, if $n_e(\vec{r}, t)$ and $n_+(\vec{r}, t)$ do not appreciably change their spatial forms during the afterglow, and if NO^+ ions and electrons are removed in equal numbers from the plasma, so that $n_+(\vec{r}, t) \approx n_e(\vec{r}, t) = R(\vec{r})T(t)$, then

$$\vec{\Gamma}_{\text{wall}}^+ = -D_a [\Delta R(\vec{r})]_{\text{wall}} T(t) = aT(t), \quad (4)$$

where a is a constant. Also, with this assumption the field-weighted average electron density may be expressed as

$$\bar{n}_{\mu w} = \frac{\int_V E_0^2(\vec{r}) R(\vec{r}) dV}{\int_V E_0^2(\vec{r}) dV} T(t) = a' T(t), \quad (5)$$

where a' is a constant. Thus $\vec{\Gamma}_{\text{wall}}^+$ and $\bar{n}_{\mu w}$ will have the same time dependence under these conditions. Now both electron-ion recombination and ambipolar diffusion remove NO^+ ions and electrons

in equal numbers. Once it is established from the temporal form of the decay of $\bar{n}_{\mu W}$ that recombination is the dominant electron-removal process, i. e., a "recombination solution" is obeyed (see Sec. IV), then the similar time dependence of $\bar{n}_{\mu W}$ and $\bar{\Gamma}_{\text{wall}}^+$, so-called "tracking", is an excellent verification that one is measuring the recombination rate between electrons and the identified ion species.

III. ATTACHMENT AND DIFFUSION STUDIES

In an early version of the apparatus without mass analysis, measurements of the rates of three-body electron attachment and ambipolar diffusion were carried out in pure NO. In the attachment process, a free electron reacts with a NO molecule, probably to form the negative ion NO^- with a second NO molecule to stabilize the reaction. Schematically, this is represented by



The rate at which electron attachment alters the electron density is then proportional to the product of the densities of the reactants (the NO molecules and the electrons). This may be written as

$$\partial n_e / \partial t = -K n^2(\text{NO}) n_e = -\nu_A n_e, \quad (7)$$

where $n(\text{NO})$ is the NO molecule density, K is the three-body attachment coefficient, and ν_A is the attachment loss frequency.

Ambipolar diffusion is a transport process in which NO^+ ions and electrons flow from the plasma to the walls of the containing vessel. It can be shown that late in the afterglow only "fundamental mode" diffusion need be considered. The loss rate of electron (and ion) concentration may then be expressed by

$$\partial n_e / \partial t = -(D_a / \Lambda_f^2) n_e = -\nu_D n_e, \quad (8)$$

where D_a is the ambipolar diffusion coefficient, Λ_f is the fundamental mode diffusion length,⁸ and ν_D is the diffusion loss frequency. It can be shown that D_a , and therefore ν_D , is inversely proportional to the NO pressure. Therefore, late in the afterglow the electron decay at each point in space is given by

$$n_e(\vec{r}, t) / n_e(\vec{r}, 0) = e^{-(\nu_A + \nu_D)t}. \quad (9)$$

Since the spatial form of the electron density remains constant, $\Delta f(t)$ is simply proportional to $n_e(\vec{r}, t)$.

In our earliest experiments, the photoionizing lamp was repetitively pulsed at about 40 Hz. As the repetition frequency was decreased, the electron loss frequency ν was found to decrease. This effect presumably resulted from a reduced accumulation of negative ions as the pulse rate was decreased, leading to a reduction in the enhanced electron diffusion caused by negative ions.⁹ As

a result, all further data were taken with the "single-pulse" method, in which a single point of the n_e versus t curve is taken from a single-pulse afterglow, with at least 10 sec between pulses. It was found that the measurements were affected by the buildup of negative ions even during the single-pulse afterglow. Empirically this effect was minimized by reducing the photoionization intensity to the lowest practicable value.

Examples of the "single-pulse" data obtained under conditions of minimal negative-ion influence are plotted as shown in Fig. 2. The frequency

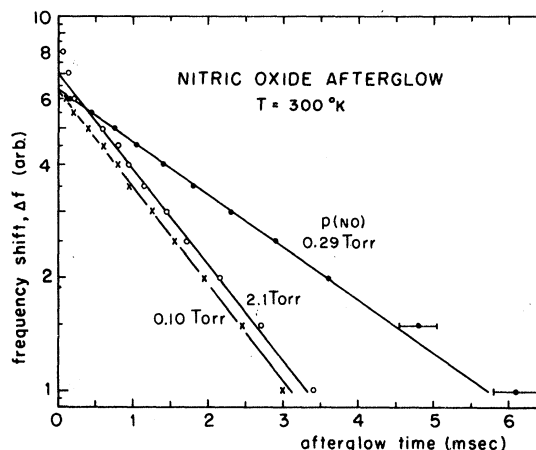


FIG. 2. Measured electron-density decays in pure NO, resulting from attachment and diffusion loss.

shift Δf is plotted vertically on a logarithmic scale; the afterglow time is plotted horizontally on a linear scale. After a brief period in which the higher diffusion modes decay, the data points fall on a straight line on the semilog plot, whose slope is the total loss frequency ν . At the lowest pressure, $p(\text{NO}) = 0.10$ Torr, diffusion is dominant. As the pressure is increased to $p(\text{NO}) = 0.29$ Torr, the diffusion loss decreases and therefore, the slope ν of the decay curve decreases. As the pressure is further increased to $p(\text{NO}) = 2.1$ Torr, attachment becomes dominant and the loss frequency increases.

The total loss frequency behaves as

$$\nu = \nu_D + \nu_A = A/p + Bp^2, \quad (10)$$

where A and B are constants. A convenient way of presenting the variation of electron loss frequency with pressure is the log-log plot of Fig. 3. The solid line through the data is not a best fit to the data, but is a curve following the pressure variation form of Eq. (10). From the values of A and B derived from the fit, the coefficients $K = 1.3 \times 10^{-31}$ cm⁶/sec and $(D_a p) = 80$ cm² Torr/sec are obtained. In the diffusion-controlled data ($p \lesssim 0.5$ Torr) of Fig. 3 some of the points lie above the line of slope -1 by $\sim 50\%$. This may be due to some residual negative-ion effect. A further possibility comes from the discovery of the presence of the dimer ion $(\text{NO})_2^+$ at these NO gas

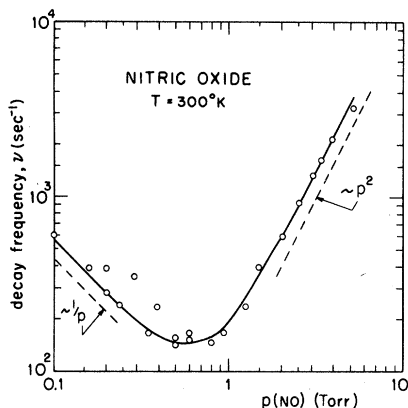


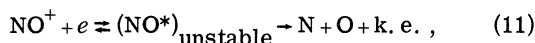
FIG. 3. Measured decay frequencies in pure NO at various pressures using "single-pulse" ionization and lowest initial electron densities. The solid line through the data is a curve of the form $A/p + Bp^2$, the expected form for combined attachment and diffusion loss.

pressures in a later apparatus with mass analysis. The NO^+ ion may be expected to diffuse less rapidly than the $(\text{NO})_2^+$ ion, since the NO^+ ion undergoes resonant charge exchange with an NO molecule. An experiment with an appreciable concentration of $(\text{NO})_2^+$ ions present in the late afterglow could then exhibit the larger diffusion loss noted.

Considering the uncertainties in determinations of NO pressures, afterglow time, and decay constant, the deduced value of the three-body electron attachment coefficient is $K = (1.3 \pm 0.1) \times 10^{-31} \text{ cm}^6/\text{sec}$ and the ambipolar diffusion coefficient is $(D_a p) = 80 \pm 16 \text{ cm}^2 \text{ Torr}/\text{sec}$ at 300°K .

IV. RECOMBINATION STUDIES

Recombination of electrons with NO^+ ions involves the dissociative capture process. The electron is captured (in a radiationless transition) by the NO^+ ion to form an unstable state of the excited molecule. If the electron is not released by auto-ionization, the molecule dissociates into a nitrogen and an oxygen atom, thus removing the excess energy of the reaction as kinetic energy (k. e.). Schematically, this is represented by



where the superscripts $+$ and $*$ refer to ionized and excited states, respectively. The rate at which dissociative recombination reduces the electron density is proportional to the product of the densities of the reactants (the NO^+ ions and electrons). This may be written as

$$\partial n_e / \partial t = -\alpha n_+ n_e \approx -\alpha n_e^2, \quad (12)$$

where n_+ is the NO^+ ion density and α is the two-body recombination coefficient. If there is only one positive-ion species and no negative ions present, quasineutrality requires that the NO^+ ion density approximately equal the electron density, leading to the approximation given by the right-

hand member of Eq. (12).

In order to obtain approximate solutions for $\bar{n}_{\mu\text{W}}(t)$, we make use of the empirical observation from nitrogen-neon and neon afterglow studies^{10,11} that the form of the spatial distribution of electrons and ions does not change appreciably during much of the afterglow. Assuming a constant spatial form, i. e., $n_e(\vec{r}, t) = R(\vec{r})T(t)$, it can be shown¹⁰ that Eq. (12) yields the solution

$$1/\bar{n}_{\mu\text{W}}(t) = 1/\bar{n}_{\mu\text{W}}(0) + C\alpha t, \quad (13)$$

where $C = [\int_V R^2(\vec{r})dV / \int_V R(\vec{r})dV][\int_V E_0^2(\vec{r})dV /$

$$\int_V R(\vec{r})E_0^2(\vec{r})dV]. \quad (14)$$

Thus, if the reciprocal of $\bar{n}_{\mu\text{W}}$ is plotted as a function of afterglow time, a straight line of slope, $S = C\alpha$, is expected if recombination is the dominant loss process.

Evaluation of the constant C , Eq. (14), requires knowledge of the initial electron spatial distribution produced by the photo-ionizing radiation from the hydrogen lamp. The problem of using this ionization source, which falls off in the axial z direction and varies in intensity with radius, together with the loss processes of recombination and diffusion, to determine an initial electron spatial distribution is extremely complicated. When enough assumptions and approximations are made to make the problem tractable, the results are of questionable value, at least for purposes of accurate ($\pm 10\%$) determinations of α .

The problem of the initially asymmetric plasma distribution was overcome, with some decrease in the linear range of $1/\bar{n}_{\mu\text{W}}$ versus t data, by using a higher diffusion rate (the neon-buffer gas pressure was reduced). As a result, the electrons and ions diffuse a distance comparable to the fundamental diffusion length of the cavity in a fraction of a typical photoionization pulse period. Consequently the electron (and ion) distribution closely approaches the fundamental-mode diffusion distribution by the beginning of the afterglow.

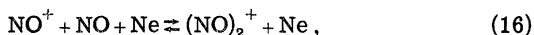
Accurate values of α are obtained from the data by computer solution¹¹ of the electron continuity equation with the ambipolar diffusion term included, i. e.,

$$\partial n_e(\vec{r}, t) / \partial t = -\alpha n_e^2(\vec{r}, t) + D_a \nabla^2 n_e(\vec{r}, t). \quad (15)$$

The computer program divides the cavity into a number of cells and obtains solutions of Eq. (15) for each cell for chosen values of α , D_a , and the central electron density at $t = 0$. An initial fundamental mode diffusion distribution (as discussed above) has been used for the computer analysis. The program then uses the computed electron densities together with the microwave electric field distribution to generate $1/\bar{n}_{\mu\text{W}}$ as a function of time. Since the diffusion coefficient and the initial central density for each experiment are known, the recombination coefficient α is the only parameter. By comparing a set of $1/\bar{n}_{\mu\text{W}}$ versus t

curves for various α 's with the experimental data, the value of α is determined.

Our early recombination experiments were carried out with $p(\text{NO}) \sim 0.1$ Torr and $p(\text{Ne}) \sim 30$ Torr. The dominant ions observed were NO^+ , which was expected, and the NO dimer ion $(\text{NO})_2^+$, which was unexpected. The $(\text{NO})_2^+$ ions were probably formed from the NO^+ ions through the reaction,



where the Ne atom removes the energy of association. At the higher partial pressures of NO, the $(\text{NO})_2^+$ ion wall current was greater than the NO^+ ion wall current. As the partial pressure of NO was reduced, the ratio of the $(\text{NO})_2^+$ current to the NO^+ current decreased, until at a few mTorr only the NO^+ ion was observed. NO^+ and $(\text{NO})_2^+$ were the only positive ions observed in significant amounts at all pressures. At high partial pressures of NO, trace amounts of NO_2^+ and an ion of mass 66, possibly NeNO_2^+ , were observed. NO_2^- was the only negative ion observed, except for a trace of Cl^- .

It was also noted that the rate of decay of electron density decreased as the ratio of $(\text{NO})_2^+$ to NO^+ decreased, and then became fairly constant when only NO^+ was observed. This implies that the $(\text{NO})_2^+$ ion has a larger recombination coefficient than the NO^+ ion. Therefore, any determinations of the NO^+ recombination rate should be made under conditions where only NO^+ is observed, i. e., at very low partial pressures of NO.

A. NO^+ Results

An example of the data obtained at $T = 300^\circ\text{K}$ is shown in Fig. 4. Figure 4(a) presents $1/\bar{n}_{\mu\text{W}}$ versus

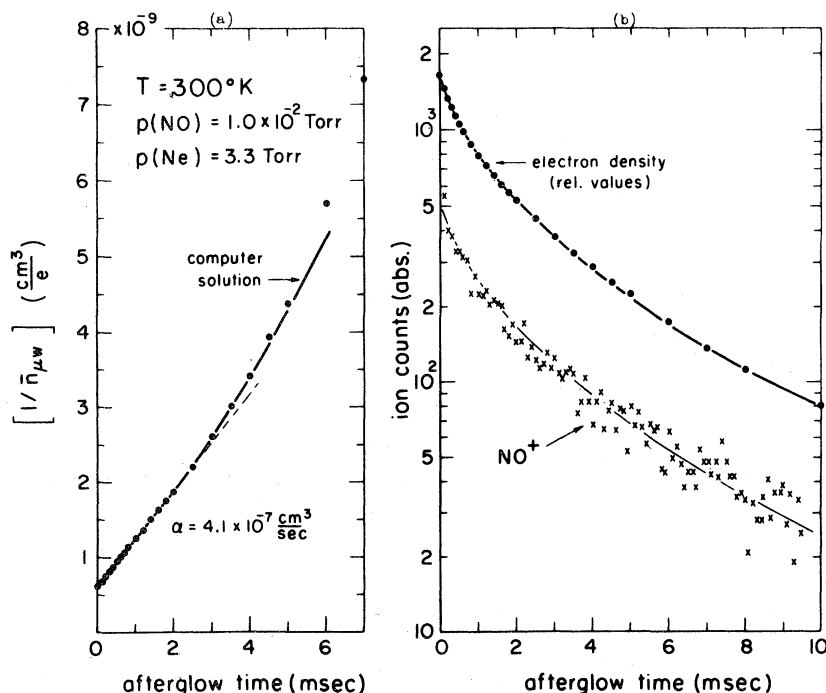


FIG. 4. Recombination loss of electrons and NO^+ ions at $T = 300^\circ\text{K}$. (a) The solid line is the computer solution for $\alpha = 4.1 \times 10^{-7} \text{ cm}^3/\text{sec}$. (b) The dashed line through the NO^+ ion wall current is the electron-density curve renormalized; the NO^+ ion current decay is seen to track the electron-density decay.

time (recombination plot); the points are the experimental data. The solid line is the computer-generated curve for a value $\alpha = 4.1 \times 10^{-7} \text{ cm}^3/\text{sec}$. Our measured value $D_{\text{eff}} = 580 \pm 60 \text{ cm}^2 \text{ Torr}/\text{sec}$ has been used for the ambipolar diffusion of NO^+ ions and electrons in neon. The experimental data follow a straight line to about $t = 3$ msec and then curve upward due to diffusion, in agreement with the computer solution. The effect of diffusion appearing in the data after only a factor of 4 in density decay is the price of using a high diffusion rate in order to improve the form of the initial electron spatial distribution. At $t = 6$ msec the experimental data lie above the computer solution, probably due to increased diffusion resulting from some accumulation of negative ions. In Fig. 4(b) the ion wall current curve and the $\bar{n}_{\mu\text{W}}$ curve are plotted on a semilogarithmic scale. The dashed line through the NO^+ curve is the $\bar{n}_{\mu\text{W}}$ curve renormalized; the NO^+ current is seen to track the electron density.

In view of this tracking and the fact that only NO^+ ions are observed, it is clear that it is recombination between NO^+ ions and electrons that is occurring with a coefficient $\alpha = 4.1 \times 10^{-7} \text{ cm}^3/\text{sec}$. Five other measurements at $T = 300^\circ\text{K}$ with various pressures of NO and Ne yield the same results as the example of Fig. 4, with the only ion present, NO^+ , tracking the electron density and a computer-generated solution for $\alpha = 4.1 \times 10^{-7} \text{ cm}^3/\text{sec}$ fitting the experimental data well. The range of NO pressure is approximately 5–41 mTorr; below this range the initial electron density is too low for good recombination control of the afterglow, and above this range the dimer ion $(\text{NO})_2^+$ begins to appear. These α values show no dependence on the NO pressure, Ne pressure, or the initial electron density, which is further assurance that no

other electron loss process is interfering with the determinations of the recombination coefficient.

To study recombination at an electron-ion-neutral-gas temperature of 450°K, the cavity is insulated and heated, the temperature of the cavity being measured with a thermocouple. An example of the data obtained at $T = 450^\circ\text{K}$ is shown

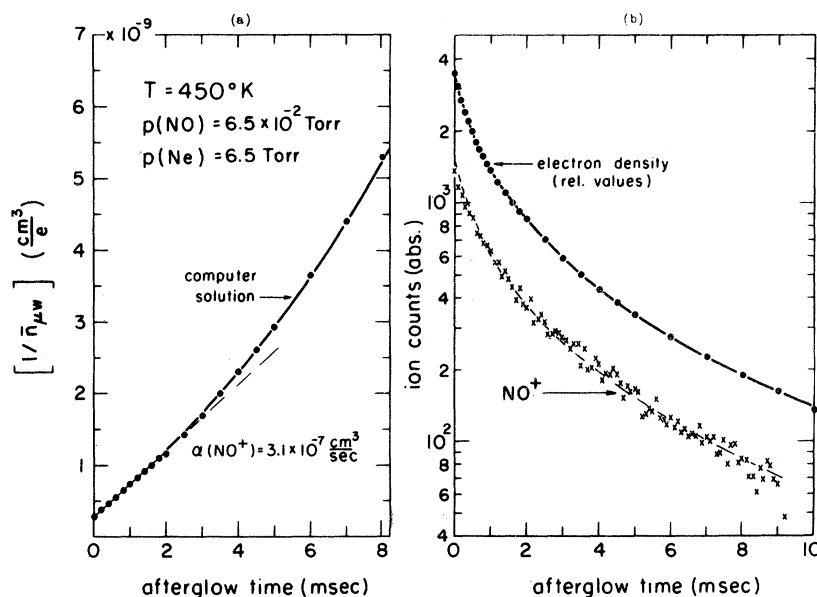


FIG. 5. Recombination loss of electrons and NO^+ ions at $T = 450^\circ\text{K}$. (a) The solid line is the computer solution for $\alpha = 3.1 \times 10^{-7} \text{ cm}^3/\text{sec}$. (b) The dashed line through the NO^+ -ion wall current is the electron-density curve renormalized; the NO^+ -ion-current decay is seen to track the electron-density decay.

the semilogarithmic plot of the ion wall current curve and the $\bar{n}_{\mu\text{W}}$ curve. The only ion observed, NO^+ , is seen to track the electron density. Again, five other experiments at $T = 450^\circ\text{K}$ with various pressures of NO and Ne yield the same results as the example of Fig. 5, with the only ion present, NO^+ , tracking the electron density, and a computer-generated solution for $\alpha \approx 3.1 \times 10^{-7} \text{ cm}^3/\text{sec}$ fitting the experimental data quite well. It was noted that at 450°K the dimer ion, $(\text{NO})_2^+$, first appeared at higher NO pressures than at $T = 300^\circ\text{K}$. Again, the α values show no dependence on the NO pressure, the Ne pressure, or the initial electron density.

To study recombination at an electron-ion-neutral-gas temperature of 200°K, the cavity is cooled with dry ice. The rate of formation of the dimer ions, $(\text{NO})_2^+$, showed a great increase at $T = 200^\circ\text{K}$ compared to $T = 300$ and 450°K . The $(\text{NO})_2^+$ problem was so serious that in only one pair of experiments, at $p(\text{NO}) = 12 \text{ mTorr}$, was NO^+ the only ion observed while a sufficiently large initial electron density was obtained for recombination control. One of these two pieces of data obtained at $T = 200^\circ\text{K}$ is shown in Fig. 6. In the recombination plot, Fig. 6(a), the experimental data follow the computer-generated solution for a factor of about 4 and then deviate upward. The upward deviation is possibly the influence of an increasingly significant concentration of the dimer ion $(\text{NO})_2^+$ whose recombination coefficient is greater than that of NO^+ . In Fig. 6(b) the NO^+ current tracks the electron density for about the first 3 msec and then begins to decay somewhat

more rapidly. If the total positive-ion density remains approximately equal to the electron density, $n(\text{NO}^+) + n((\text{NO})_2^+) \approx n_e$, then the more rapid decay of the NO^+ current after 3 msec may indicate an increasingly significant density of $(\text{NO})_2^+$, as suggested previously by the appearance of the recombination plot. The period in which the NO^+ current tracks the electron density is approximately the period in which the computer solution for $\alpha = 7.4 \times 10^{-7} \text{ cm}^3/\text{sec}$ is a good fit to the data. Therefore, this value is taken as $\alpha(\text{NO}^+)$. The data of another experiment are similar to those of Fig. 6, with a computer-generated curve for $\alpha = 7.8 \times 10^{-7} \text{ cm}^3/\text{sec}$ fitting the data fairly well. A slight margin of confidence is given to the data of Fig. 6, with the result that the recombination coefficient of NO^+ ions and electrons at $T = 200^\circ\text{K}$ is taken to be $\alpha = 7.4 \times 10^{-7} \text{ cm}^3/\text{sec}$.

B. $(\text{NO})_2^+$ Results

The results of the early experiments in which the $(\text{NO})_2^+$ ion was observed can be used to determine approximately the recombination coefficient of the $(\text{NO})_2^+$ ion. If, as a result of rapid equilibration between the $(\text{NO})_2^+$ and the NO^+ ions, the ratio of the ion densities is constant, and we use quasi-neutrality of the plasma afterglow,

$$n_e \approx n(\text{NO}^+)(1 + \lambda), \quad (17)$$

where $\lambda = n((\text{NO})_2^+)/n(\text{NO}^+)$, Eq. (12) then becomes

$$\frac{dn_e}{dt} = -[(\alpha_1 + \lambda\alpha_2)/(1 + \lambda)]n_e^2 = -\alpha_{\text{eff}}n_e^2, \quad (18)$$

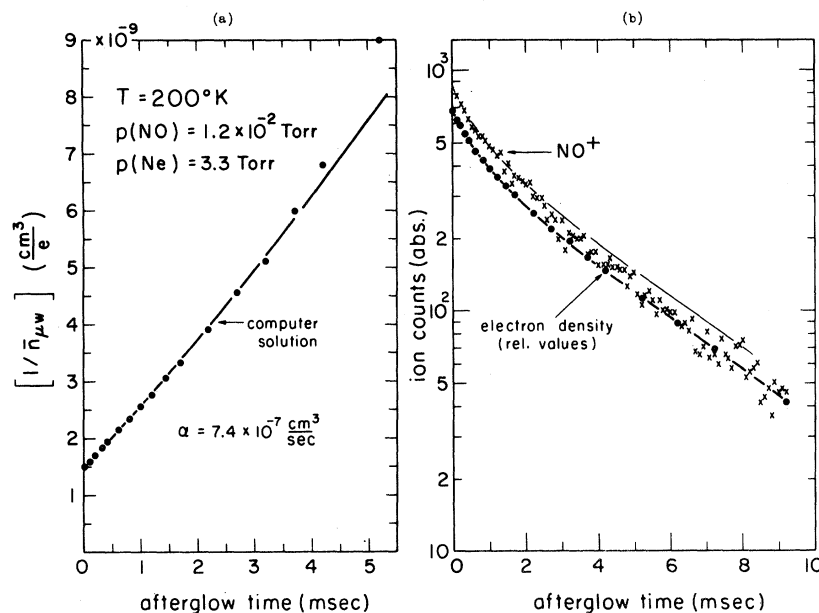


FIG. 6. Recombination loss of electrons and NO^+ ions at $T = 200^\circ\text{K}$. (a) The solid line is the computer solution for $\alpha = 7.4 \times 10^{-7} \text{ cm}^3/\text{sec}$. (b) The dashed line through the NO^+ -ion wall current is the electron-density curve renormalized; the NO^+ -ion-current decay is seen to track the electron-density decay for the first 3 msec.

where α_1 and α_2 are the recombination coefficients of the NO^+ and $(\text{NO})_2^+$ ions, respectively. The form of Eq. (18) suggests introduction of an effective recombination coefficient,

$$\alpha_{\text{eff}} = (\alpha_1 + \lambda\alpha_2)/(1 + \lambda). \quad (19)$$

The expression for the ion wall current previously developed, Eq. (3), is for electrons and a single positive-ion species; for electrons and two positive-ion species similar expressions are valid. Since the diffusion coefficients of the ions are, in general, different, the ratio of ion densities in the cavity, λ , will not equal the ratio of wall currents, R . Furthermore, electron multipliers are known to have different secondary emission characteristics for different ions.¹² There also is the possibility that a weakly bound molecule such as $(\text{NO})_2^+$ may be broken up by a collision while being accelerated into the mass filter. To allow for such problems, a sampling efficiency factor, F , is introduced, defined by $\lambda \equiv FR$. Then Eq. (19) becomes

$$\alpha_{\text{eff}} = (\alpha_1 + FR\alpha_2)/(1 + FR). \quad (20)$$

An example of the dimer-controlled recombination data which was obtained is shown in Fig. 7(a). The gas pressures are $p(\text{NO}) = 200$ mTorr and $p(\text{Ne}) = 15$ Torr and the temperature is 300°K . On the recombination plot, the experimental data are seen to follow a straight line, as would be expected for recombination control, from $0.6 \leq t \leq 2.6$ msec with a slope of $S = 35 \times 10^{-7} \text{ cm}^3/\text{sec}$. In Fig. 7(b) the ion wall currents and $\bar{n}\mu_w$ are plotted semi-logarithmically. The NO^+ current, initially greater than the $(\text{NO})_2^+$ current, quickly decays to the equilibrium value, and the $(\text{NO})_2^+$ current becomes dominant at about 0.7 msec. This is due to conversion of the NO^+ ions to $(\text{NO})_2^+$ ions through reaction (16). In Fig. 7(b), the dashed

line through the $(\text{NO})_2^+$ current is just the $\bar{n}\mu_w$ curve renormalized. Thus it is the $(\text{NO})_2^+$ ion that "tracks" the electron density from $t = 0.6$ to $t \approx 3$ msec, the period in which the recombination plot is a straight line. Therefore the recombination coefficient α , corresponding to the slope S , in this plot would be almost entirely due to recombination of electrons with $(\text{NO})_2^+$ ions.

As the partial pressure of NO is decreased while keeping the Ne pressure constant, the recombination slope S and the relative importance of $(\text{NO})_2^+$ with respect to NO^+ also decrease, until a point is reached at which the slope remains fairly constant and the only ion detectable is NO^+ . This constant slope, $S = 9.0 \times 10^{-7} \text{ cm}^3/\text{sec}$, corresponds to the established value of the NO^+ recombination coefficient $\alpha(\text{NO}^+) = 4.1 \times 10^{-7} \text{ cm}^3/\text{sec}$ at $T = 300^\circ\text{K}$. The constant C in Eq. (13) is therefore equal to 2.2. This value is reasonable, since the C value of the experiments at the low neon pressures discussed earlier is 1.5. Furthermore, a calculation of C for these high neon pressure experiments, using a crude model of the initial electron distribution, gives a value of 2.1. If C is assumed constant, then we may evaluate α_{eff} from the slopes S of curves of the type shown in Fig. 7 by use of the equation

$$\alpha_{\text{eff}} = S/2.2. \quad (21)$$

In the data from these experiments, the ratio of the observed wall currents, $R = (\text{NO})_2^+/\text{NO}^+$, remains fairly constant in the afterglow period when the recombination plot is a straight line, supporting the equilibrium density assumption used in deriving Eq. (19).

In Fig. 8, the effective recombination coefficients α_{eff} derived from Eq. (21) are plotted versus R , the ratio of the observed wall currents. The data proceed from a value of $\alpha_{\text{eff}} = 4.1 \times 10^{-7} \text{ cm}^3/\text{sec}$ for essentially no observed $(\text{NO})_2^+$ ions

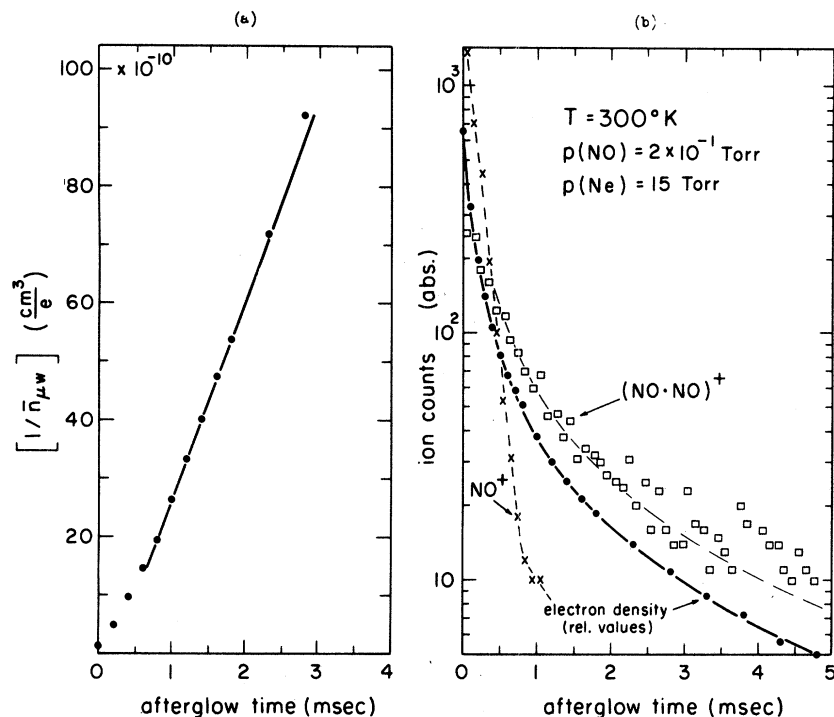


FIG. 7. Recombination loss of electrons at $T=300^\circ\text{K}$. (a) The straight line corresponds to an $\alpha_{\text{eff}} = 1.6 \times 10^{-6} \text{ cm}^3/\text{sec}$. (b) The $(\text{NO})_2^+$ -ion current is seen to track the electron-density decay for the period that the recombination plot follows a straight line.

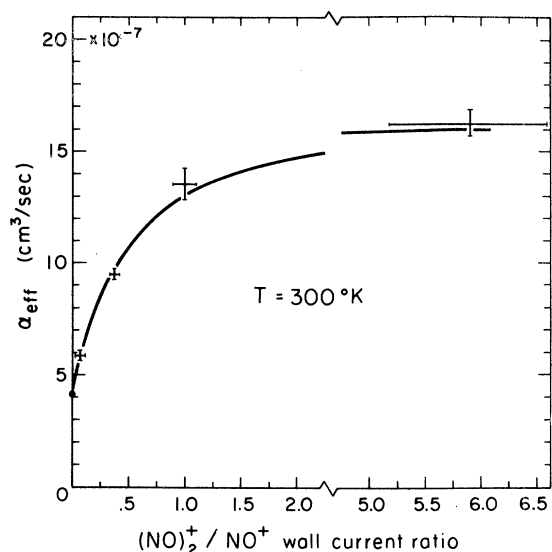


FIG. 8. Measured effective recombination coefficient for various ion wall current ratios $(\text{NO})_2^+ / \text{NO}^+$. The solid line through the data is the expected theoretical dependence of α_{eff} on the ion wall current ratio.

up to approximately $\alpha_{\text{eff}} = 1.6 \times 10^{-6} \text{ cm}^3/\text{sec}$ for $R = 6$. The predicted variation of α_{eff} with R , Eq. (20), with parameters $\alpha_2 = 1.7 \times 10^{-6} \text{ cm}^3/\text{sec}$ and $F = 2.2$, is indicated by the solid curve in Fig. 8, and is seen to provide a good fit to the data. Therefore, it is concluded that at $T = 300^\circ\text{K}$ the $(\text{NO})_2^+$ ion recombination coefficient is $\alpha[(\text{NO})_2^+] \approx 1.7 \times 10^{-6} \text{ cm}^3/\text{sec}$. Furthermore, the inferred value $F = 2.2$ for the relative sampling efficiency suggests that nothing very drastic is

occurring in the ion sampling process.

The principal uncertainty in determining the values of the NO^+ recombination coefficient arises in fitting the computer solutions of the continuity equation to the experimental data. Computer curves with α values slightly different than the α value of the "best fit" computer curve can still satisfactorily fit the data. This results in an approximate $\pm 5\%$ uncertainty in the value of α . Systematic errors in measurements of frequency shift and afterglow time probably are $\sim 1\%$. Therefore, we assign values for the recombination coefficient of electrons and NO^+ ions of $\alpha(\text{NO}^+) = (7.4 \pm 0.7)$, (4.1 ± 0.3) , and $(3.1 \pm 0.2) \times 10^{-7} \text{ cm}^3/\text{sec}$ at $T = 200$, 300 , and 450°K , respectively. Considering the uncertainties in the value of $\alpha(\text{NO}^+)$ and in the experimentally determined ratio of $\alpha(\text{NO}^+) / \alpha((\text{NO})_2^+)$, we assign a value for the recombination coefficient of electrons and $(\text{NO})_2^+$ ions of $\alpha((\text{NO})_2^+) = (1.7 \pm 0.4) \times 10^{-6} \text{ cm}^3/\text{sec}$ at $T = 300^\circ\text{K}$.

It is customary to attempt to assign a power-law temperature dependence, T^{-N} , to the recombination coefficient, although such simple temperature dependences only occur under rather special circumstances.¹³ A T^{-1} dependence can be fit to the $\alpha(\text{NO}^+)$ determinations, but it appears forced, and the results are felt to be more accurate than this would imply. Actually, the recombination coefficient apparently varies more rapidly with temperature between 200 and 300°K than between 300 and 450°K .

V. DISCUSSION

The recent literature contains several studies of electron loss processes in NO. Gunton and Shaw¹⁴ (GS) photoionized (using "single pulses" of $\lambda = 1216 \text{ \AA}$ radiation) purified NO and NO-Ne mixtures

within a 10-GHz microwave cavity and used a microwave technique to measure the electron-density decay. They utilized a differentially pumped mass spectrometer, and at low gas pressures observed only NO^+ and NO_2^+ ions; unfortunately, their mass spectrometer did not function under the higher gas pressure conditions of the recombination measurements. GS also noticed the decrease in the apparent recombination coefficient with decreasing NO partial pressure, but attributed it to negative-ion effects. Their value of the three-body attachment coefficient, $K = (2.2 \pm 0.2) \times 10^{-31} \text{ cm}^3/\text{sec}$, at $T = 300^\circ\text{K}$ is about 70% greater than that of the present experiment; in this case, the lower value (present results) should more nearly represent the correct value, since negative-ion effects increase the apparent attachment rate. Their value of $D_0p = 83 \pm 8 \text{ cm}^2 \text{ Torr}/\text{sec}$ at $T = 300^\circ\text{K}$ agrees well with the present value. Without simultaneous ion identification, GS found values of the NO^+ recombination coefficient of $\alpha = (10 \pm 2)$, (4.6 ± 0.5) , and $(3.5 \pm 0.2) \times 10^{-7} \text{ cm}^3/\text{sec}$ at $T = 196$, 298, and 358°K , respectively. Their values at $T = 298$ and 358°K agree with the present results; that at $T = 196^\circ\text{K}$ is somewhat higher, probably due to the influence of the dimer ion $(\text{NO})_2^+$.

Young and St. John¹⁵ (YS) used chemi-ionization in mixtures of N, O, and N_2 to produce NO^+ ions. With this method of ionization, neutral NO molecules were not present, so there was the apparent advantage of being free of $(\text{NO})_2^+$ ion formation. However, there was no mass analysis to identify the dominant ion. Currents arriving at the pulsed collector electrodes were used to measure the rate of growth and the equilibrium value of the density. YS assumed that in their experiments NO^+ was the dominant ion, that there were no negative ions present, that there were no other loss processes (such as diffusion) occurring, and that

the ion and electron densities were spatially uniform. They obtained a value of the NO^+ recombination coefficient of $(5 \pm 2) \times 10^{-7} \text{ cm}^3/\text{sec}$ at $T = 300^\circ\text{K}$; the present, more accurately determined value lies within this range.

In an early experiment to measure the recombination rate of NO^+ , Doering and Mahan¹⁶ photoionized (using $\lambda = 1236 \text{ \AA}$ radiation) purified NO gas in an apparatus without mass analysis. From negative probe currents at equilibrium ion density, they estimated an upper limit of the recombination coefficient of $2 \times 10^{-6} \text{ cm}^3/\text{sec}$. From positive probe currents from a decaying plasma they obtained a range of values for the recombination coefficient from 2×10^{-7} to $1.4 \times 10^{-6} \text{ cm}^3/\text{sec}$; this large range encompasses the value of the present experiment.

Mentzoni and Donohoe¹⁷ (MD) ionized unpurified NO gas with a repetitively pulsed electrical discharge. Electron-density decay was measured with a microwave technique; there was no mass analysis. Lack of ion identification was most unfortunate, considering the probable creation of many neutral and ionized species in an electrical discharge in NO, accompanied by the accumulation of negative ions. MD obtained values of the recombination coefficient from 2.6×10^{-7} to $8.0 \times 10^{-7} \text{ cm}^3/\text{sec}$, which encompass the value of the present experiment.

Thus, the present results provide an improved determination of the recombination coefficient, $\alpha(\text{NO}^+)$ over the temperature range $200\text{--}450^\circ\text{K}$, free of interference by the dimer ion $(\text{NO})_2^+$. In addition, the dimer ion recombination coefficient, $\alpha((\text{NO})_2^+)$, has been measured for the first time.

The authors wish to thank L. Frommhold for his assistance with the computer solutions of the electron continuity equation.

*This research was supported, in part, by the Army Research Office-Durham, (DA-ARO-D-124-0965).

†Present address: E. O. Hulburt Center for Space Research, U. S. Naval Research Laboratory, Washington, D. C.

¹T. M. Donahue, *Science* **159**, 489 (1968).

²C. Y. Johnson in *Annals of the International Quiet Solar Year*, edited by C. M. Minnis (Massachusetts Institute of Technology Press, Cambridge, Mass., to be published), Vol. 5.

³U. S. Standard Atmosphere Suppl. (U. S. Government Printing Office, Washington, D. C., 1966).

⁴N. W. Spencer, L. H. Brace, G. R. Carnigan, D. R. Tausch, and H. Nieman, *J. Geophys. Res.* **70**, 2665 (1965).

⁵M. A. Biondi, *Rev. Sci. Inst.* **22**, 500 (1951).

⁶W. Paul and M. Raether, *Z. Physik* **140**, 262 (1955).

⁷Manufactured by the Bendix Corp., Southfield, Michigan.

⁸M. A. Biondi and S. C. Brown, *Phys. Rev.* **75**, 1700 (1949).

⁹M. A. Biondi, *Phys. Rev.* **109**, 2005 (1958).

¹⁰W. H. Kasner and M. A. Biondi, *Phys. Rev.* **137**, A317 (1965).

¹¹L. Frommhold, M. A. Biondi, and F. J. Mehr, *Phys. Rev.* **165**, 44 (1968).

¹²B. L. Schram, A. J. H. Boerboom, W. Kleine, and J. Kistemaker, *Physica* **32**, 749 (1966).

¹³*Atomic and Molecular Processes*, edited by D. R. Bates (Academic Press, Inc., New York, 1962).

¹⁴R. C. Gunton and T. M. Shaw, *Phys. Rev.* **140**, A756 (1965).

¹⁵R. A. Young and G. St. John, *Phys. Rev.* **152**, 25 (1966).

¹⁶J. P. Doering and B. H. Mahan, *J. Chem. Phys.* **36**, 669 (1962).

¹⁷M. Mentzoni and J. Donohoe, *Can. J. Phys.* **45**, 1565 (1967).